


## ARTICLE

# A practical approach for monitoring reinforcement corrosion in steel fiber reinforced concrete elements exposed to chloride rich environments

Enzo Gomez<sup>1,2</sup> | Bruno Leporace-Guimil<sup>3</sup> | Antonio Conforti<sup>3</sup>  | Giovanni Plizzari<sup>3</sup> | Gustavo Duffó<sup>1,4,5</sup> | Raul Zerbino<sup>6,7,8</sup>

<sup>1</sup>Atomic Energy National Commission (CNEA), San Martin, Argentina

<sup>2</sup>Argentine Catholic University (UCA), Buenos Aires, Argentina

<sup>3</sup>Department of Civil, Environmental, Architectural Engineering and Mathematics (DICATAM), University of Brescia, Brescia, Italy

<sup>4</sup>National University of San Martin (UNSAM), San Martin, Argentina

<sup>5</sup>National Council for Scientific and Technical Research (CONICET), Buenos Aires, Argentina

<sup>6</sup>Multidisciplinary Training Laboratory for Technological Research (LEMIT), La Plata, Argentina

<sup>7</sup>National University of La Plata (UNLP), La Plata, Argentina

<sup>8</sup>National Council for Scientific and Technical Research (CONICET), La Plata, Argentina

## Correspondence

Antonio Conforti, Department of Civil, Environmental, Architectural Engineering and Mathematics (DICATAM), University of Brescia, Brescia, Italy.

Email: [antonio.conforti@unibs.it](mailto:antonio.conforti@unibs.it)

## Funding information

Science, Technology, and Innovation Ministry of Argentina, through the National Found for Scientific and Technological Research (FONCYT, Argentina)

## Abstract

The use of fibers in Reinforced Concrete (RC) elements changes their cracking pattern, leading to narrower and more closely spaced cracks. In addition, the presence of fibers can improve the steel-to-concrete bond behavior reducing the steel-to-concrete interface damage after cracking. Cracks and steel-to-concrete interface damage work like paths, for aggressive agents, to reach the rebar in cracking elements, reducing the initiation period of the corrosion process, and favoring the corrosion at the intersection between cracks and reinforcement. In this context, this article discusses an experimental program on tension ties mechanically cracked and exposed to a chloride-rich environment with the purpose to check and eventually adequate the typical electrochemical measurements, used in the case of RC elements, for Steel Fiber Reinforced Concrete (SFRC). Adjustments related to degradation morphology and interference of steel fibers are proposed and used on Fiber Reinforced Concrete (FRC) elements for monitoring the influence of cracks and fibers on corrosion propagation. Finally, these proposed modifications were checked and validated against the results obtained by monitoring SFRC beams in the cracked stage.

Discussion on this paper must be submitted within two months of the print publication. The discussion will then be published in print, along with the authors' closure, if any, approximately nine months after the print publication.

This is an open access article under the terms of the [Creative Commons Attribution](https://creativecommons.org/licenses/by/4.0/) License, which permits use, distribution and reproduction in any medium, provided the original work is properly cited.

© 2022 The Authors. *Structural Concrete* published by John Wiley & Sons Ltd on behalf of International Federation for Structural Concrete.

**KEYWORDS**

corrosion monitoring, corrosion potential, fibers reinforced concrete, pitting corrosion, resistivity

**1 | INTRODUCTION**

Due to the alkalinity of hydrated cement ( $\text{pH} > 12.5$ ), the reinforcement embedded in concrete develops an oxide layer, called *the passive layer*, which protects the steel from corrosion degradation.<sup>1,2</sup> The ingress of aggressive agents, such as chloride ions ( $\text{Cl}^-$ ) or carbon dioxide ( $\text{CO}_2$ ), up to the reinforcement could cause localized “pitting corrosion” or uniform dama of the passive layer, leading to the onset of corrosion.<sup>1,2</sup> To characterize the service life of a reinforced concrete (RC) structure without cracks, Tuutti<sup>3</sup> proposed the first corrosion deterioration model for uncracked concrete composed of two stages: *initiation* and *propagation*, as shown in Figure 1. Based on this model, François and Arliguie<sup>4</sup> proposed a service life model adapted for cracked concrete structures that contemplates four stages:

*Incubation*: the lapse in which the aggressive agents enter through the cracks to the reinforcement destroying the *passive layer* and initiating corrosion at the zone of influence of the crack;

*Initiation*: interval which contemplates the initial development of active corrosion at the zone of influence of the crack;

*Induction*: where the development of active corrosion at the zone of influence of the crack is attenuated by the accumulation of corrosion products that seal the cracks and defects at the Steel–Concrete Interface (SCI);

*Propagation*: it represents the period in which corrosion develops over the full extent of the reinforcement.

In the propagation stage of both models, degradation could be accelerated by the formation of cracks induced by accumulated expansive corrosion products (i.e., cracks in the clear cover coinciding with the position of the reinforcements), or by the spalling of the nominal cover in a very advanced state of deterioration. In the case of cracked concrete, the accumulation of corrosion products could lead to further opening of existing cracks or the formation of new ones.

There are different strategies that allow mitigating the progress of the corrosion process during the propagation stage. In addition to the correct design, selection of materials, casting process and curing period, monitoring, and evaluation of the structures during their service life are important aspects when planning maintenance and repair strategies, or establishing the end of the service life of a civil structure.<sup>1,2</sup> Currently, there are different techniques and measurement instruments that

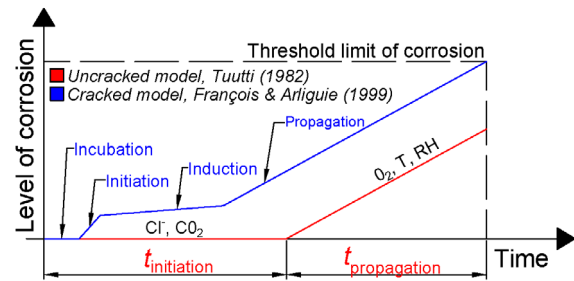


**FIGURE 1** Service life models for reinforced concrete in uncracked<sup>3</sup> and cracked stages.<sup>4</sup>

allow evaluating the progress of the corrosion process in RC structures.<sup>5,6</sup> As most of these devices were developed to evaluate conventional RC,<sup>1,5,6</sup> it is necessary to consider the possibility of adjusting the techniques, or results, if they are used in concrete with special cementitious matrices.

Particularly, chloride-induced corrosion in cracked elements is heterogeneous since it generates localized corrosion, and it is developed at the zone of influence of the cracks. The heterogeneity of the attack combined with other variables, such as environmental or loading conditions, can generate multiple deterioration scenarios even in the same structure. For decades, researchers worldwide have characterized chloride corrosion in cracked elements. One of the most studied and controversial aspects is the effect of crack width.<sup>7–10</sup> Crack direction, frequency, and depth were also studied.<sup>11,12</sup> It was established that although crack width has an influence, it has a lower impact with respect to other parameters. The morphology and cracking damage of the SCI,<sup>13,14</sup> and the exposure conditions, usually have a greater impact than crack width. However, in the long term, the limitation of crack width could mitigate the corrosion process.

The use of fibers in concrete limits the width of cracks, resulting in a greater number of cracks and lower crack spacing.<sup>15–17</sup> The presence of fibers also improves the steel–concrete bond, in terms of corrosion, some results suggest improvements in performance under certain environmental conditions<sup>18</sup> or with the use of a certain combination of fibers.<sup>7,19</sup> In particular, the presence of steel fibers affects the electrical behavior of the cementitious material,<sup>20,21</sup> which influences the electrochemical measurements of equipment used to monitor reinforcement corrosion.

**TABLE 1** Materials characteristics and mechanical properties

	Tension ties		Beams	
	RC	SF50	RC	SF25
Type of concrete				
Fibers (kg/m <sup>3</sup> )	No	Steel 50	No	Steel 25
Volume (%)		0.64		0.32
Fresh properties				
Slump (mm)	120	65	130	100
Mechanical properties				
$f_c$ (MPa)	52.1 (0.01)	52.8 (0.02)	48.3 (0.02)	48.0 (0.02)
$f_L$ (MPa)	—	5.17 (0.07)	—	4.47 (0.09)
$f_{R1}$ (MPa)	—	4.82 (0.14)	—	3.75 (0.12)
$f_{R3}$ (MPa)	—	4.89 (0.13)	—	3.28 (0.14)
Reinforcing steel				
$f_y$ (MPa)	487 (0.02)			
$f_u$ (MPa)	656 (0.01)			

However, the impact of fibers, on the corrosion of cracked elements, is not clearly known, and there is no methodology to evaluate corrosion in these types of elements. The morphology of the degradation around the crack and the influence of the steel fibers on the electrical behavior of the cementitious matrix must be considered. Therefore, clear and repeatable evaluation techniques must be defined, for which three initial problems should be considered:

1. The techniques and instrumentation, that allow quantifying the corrosion progress on ordinary concrete, are not validated in SFRC cracked element;
2. There are no evaluation methodologies that include the influence of SCI characteristics on corrosion monitoring;
3. There are no clear definitions of “allowable deterioration” in a set of rebars or individual rebar. Limit deteriorations must be established to evaluate the performance of a cementitious material at each stage.

In this context, the National University of San Martin (UNSAM—Argentina), the National University of La Plata (UNLP—Argentina), and the University of Brescia (UNIBS—Italy), with the support of the National Commission of Atomic Energy (CNEA—Argentina) and the Multidisciplinary Training Laboratory for Technological Research (LEMIT—Argentina), developed a research program to assess a methodology to monitor chloride-induced corrosion in RC and SFRC elements in the cracked stage. The program was focused on the evaluation of existing techniques and instrumentation by analyzing the interference of steel fibers in

electrochemical tests. The experimental program was carried out in two phases. The first one dealt with RC and SFRC prisms under tension. These samples are called hereafter “tension ties” and represent the part of a bent beam around reinforcement in tension. This type of specimen is often adopted to study cracking phenomena in RC elements with and without fibers.<sup>22</sup> Subsequently, a second phase was carried out on RC and SFRC beams under flexure.

## 2 | MATERIALS AND SPECIMEN GEOMETRIES

Concrete was made using CP40 cement, natural siliceous sand, and 12 mm maximum size granitic crushed stone. The water-to-cement ratio was 0.45 and a superplasticizer was incorporated to achieve adequate workability. In order to obtain two different SFRC mixtures, hooked-end steel fibers, 50 mm long and 1 mm diameter (aspect ratio 50), with a minimum tensile strength of 1100 MPa, were added to concrete. In the first phase, SFRC tension ties were made with 50 kg/m<sup>3</sup> (i.e., volume fraction 0.64%) of steel fibers while for the second one SFRC beams were produced with 25 kg/m<sup>3</sup> (i.e., volume fraction 0.32%) of steel fibers. Hereafter, both SFRC mixes will be referred to SF50 and SF25, respectively. Reinforcement bars were used “as-received” without any surface cleaning process. Material characteristics are given in Table 1, as well as fresh and hardened properties of concretes. Concerning the postcracking mechanical properties of SFRC, the mean value of the limit of proportionality ( $f_L$ ) and the residual flexural tensile strengths ( $f_{R1}$  and  $f_{R3}$  corresponding to CMOD values of 0.5 and 2.5 mm<sup>23</sup>) are summarized in Table 1 as well.

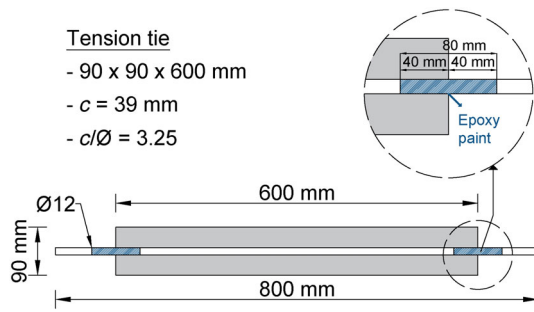


FIGURE 2 Tension ties with reinforcement details.

Eight tension ties were studied in the first phase. Four RC specimens were made with ordinary concrete while the other four were cast with SF50. The tension ties had a single reinforcement bar of  $\varnothing 12$  mm placed along the tension ties axis, a cross-sectional section of  $90 \times 90$  mm, a total length of 600 mm, a clear cover ( $c$ ) of 39 mm,  $c/\varnothing$  of 3.25, and effective reinforcement ratio  $\rho_{\text{eff}}$  1.40%, as shown in Figure 2. Before casting, the transition area of the rebar was isolated with epoxy paint to avoid crevice corrosion in the region where the reinforcement emerges from the concrete specimen. On the other hand, after cracking and before immersion in the chloride solution, the ends of the tension ties and once again the external rebar were protected with epoxy paint to avoid any deterioration of the exposed reinforcements and to guarantee that chloride only ingresses through lateral faces.

For the second phase, two RC beams with ordinary concrete, and two SF25 beams were cast. Beams were reinforced with two longitudinal bars of  $\varnothing 8$  mm placed along the tension ties axis and 6 mm stirrups placed every 50 mm. Beams had a cross-sectional section of  $150 \times 150$  mm, a total length of 900 mm, a concrete cover ( $c$ ) of 25 mm,  $c/\varnothing$  of 3.12, and a longitudinal reinforcement ratio  $\rho_s = 0.5\%$ , as shown in Figure 3. Regarding instrumentation, direct connections to the longitudinal reinforcement and adapted sensors (see Section 4) were placed at the center of the beams to monitor corrosion conditions in the cracked zone.

### 3 | PRECRACKING PHASE AND EXPOSURE CONDITIONS

Six tension ties, three in RC and three in SF50, were mechanically precracked through the uniaxial tensile test at different load levels. The latter was selected associated with the yield tensile strength ( $f_y$ ) of the rebars:  $0.9 f_y$  (51 kN),  $1.0 f_y$  (55 kN), and  $1.1 f_y$  (61 kN). The remaining tension tie of each group (one of RC and one of SF50) was kept uncracked. Table 2 shows the adopted

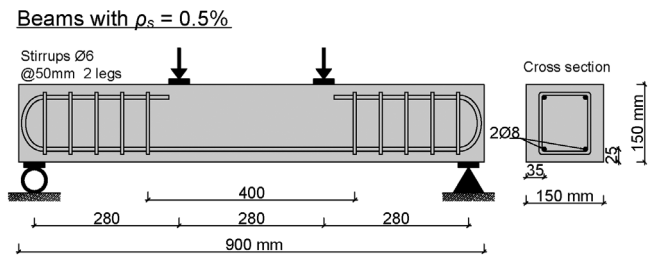


FIGURE 3 Geometry of RC beams and reinforcement details.

nomenclature for the tension ties according to the type of concrete and load levels.

The mechanical behavior of tension ties showed a clear difference between the RC and SF50 specimens, as expected.<sup>17</sup> In Figure 4, the theoretical response of a  $\varnothing 12$  mm rebar subjected to a uniaxial tensile test up to the yielding load is reported in red color, while black and grayscale colors represent the mechanical performance of the specimens at different loading levels. It can be observed that the overall uncracked branch remains similar between RC and SF50 specimens as well as the load at the first crack. In the cracked stage (both crack formation and stabilized crack stage), fibers led to a noticeable increase in the general stiffness due to the residual stresses transfer across cracks (tension softening).<sup>17</sup> In turn, the mean crack spacing of the SF50 samples resulted lower than RC samples. In general, fibers lead to a reduction in crack spacing and crack width.<sup>23</sup>

After precracking, the tension ties were pre-exposed to high-chloride sodium solution with 10% m/m of chloride ions (i.e., 165.0 g/L of NaCl) for 40 days to induce the onset of corrosion on the embedded rebar. Subsequently, specimens were subjected to wet-dry cycles using a sodium chloride solution with 3% m/m of chloride ions (i.e., 49.5 g/L of NaCl). Each cycle was carried out with an average duration of 1 month: 1 wetting week and 3 drying weeks (to cause an aggressive environment). Tension ties were exposed for 615 days (20 months) to wet-dry cycles and subsequently were opened to assess the corrosion morphology on their rebars.

Secondly, two beams in RC (i.e., RC\_A and RC\_B) and two in SF25 (i.e., SF25\_A and SF25\_B) were mechanically precracked by employing a four-point bending test. A load, associated with the maximum load ( $P_{\text{max}}$ ) established for the RC beam design in previous characterization,<sup>24</sup> was applied on all beams:  $0.45 P_{\text{max}}$  (25 kN). Figure 5 shows specimens before testing, and their mechanical performance subjected to 4 PBT. Two experimental control beams<sup>24</sup> up to the yielding load are reported in continuous and dashed red lines RC and SF25, respectively. Besides, black and gray colors depict

**TABLE 2** Summary of the experimental program on tension ties

Type of concrete	Loading levels			
	Uncracked	0.9 $f_y$ (51 kN)	1.0 $f_y$ (55 kN)	1.1 $f_y$ (61 kN)
RC	RC-UC	RC-0.9	RC-1.0	RC-1.1
SF50	SF50-UC	SF50-0.9	SF50-1.0	SF50-1.1

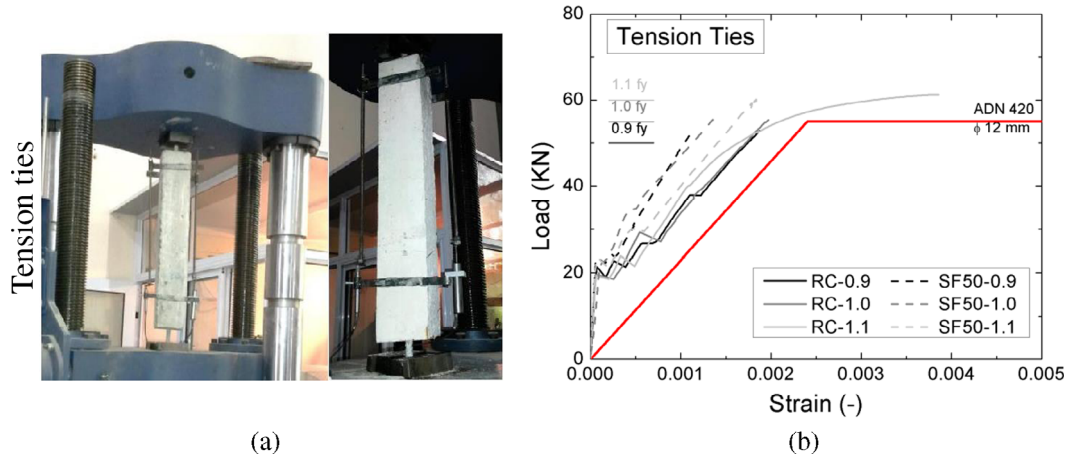


**FIGURE 4** RC and SF50 tension ties under subjected to uniaxial tensile test: specimen before testing at the Instron testing machine (a), and uniaxial load versus strain diagram (b).

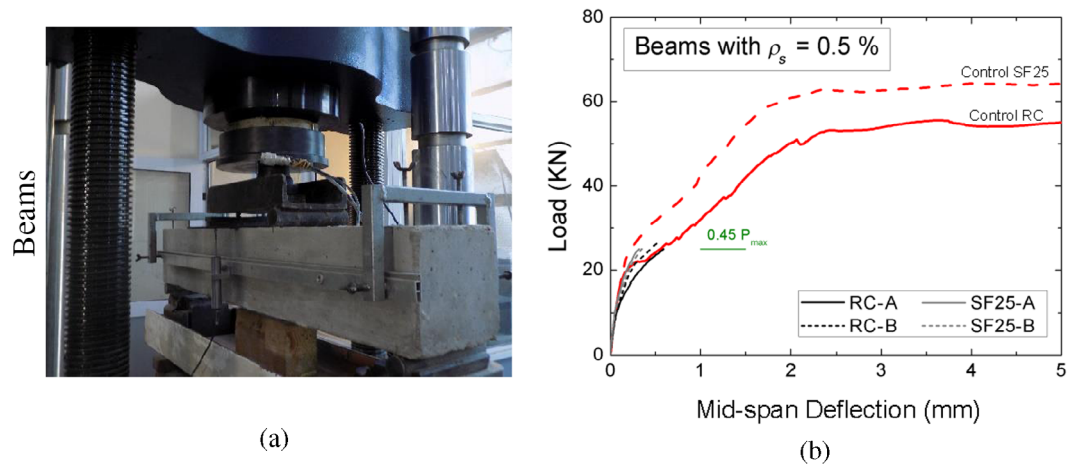


**FIGURE 5** RC and SF25 beams under 4 PBT: a beam before testing at the Instron testing machine (a), and bending load versus net deflection diagram, at the mid-span (b).

the mechanical performance of the loading of the specimen up to  $0.45 P_{\max}$  (25 kN). The mechanical behavior of Control beams (i.e., Control RC and Control SF25) until yielding load showed a clear difference between the RC and SF25 specimens regarding postcracking deflection and flexural bearing capacity. Both could be influenced by the presence of fibers in the cracking planes after the first crack.

Once the four beams were precracked, the exposure conditions repeated the steps performed for the tension ties. Currently, beams have been exposed for approximately 175 days to wet-dry cycles. For the second phase,

a target of 600 days of exposure was established, similar to the exposition of tension ties.

## 4 | CORROSION MEASUREMENTS

During the exposure to wet-dry cycles, the main electrochemical parameters, that allow characterizing the corrosion process, were monitored: corrosion current ( $I_{\text{CORR}}$ ), corrosion potential ( $E_{\text{CORR}}$ ) as well as the resistivity of the cementitious matrix ( $\rho_M$ ). A commercial Superficial Measurement Equipment (SME), with guard ring

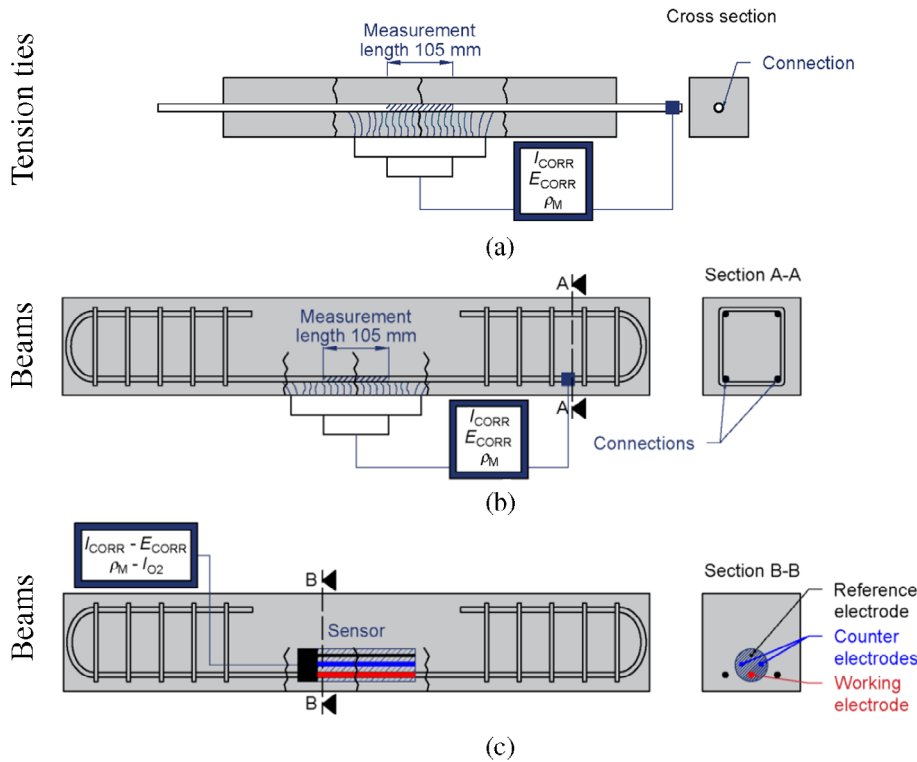


FIGURE 6 Measurement made with superficial measurement equipment (Gecor<sup>®</sup>): on tension ties (a) and beams (b), and a beam with an internal sensor (c).

technology and an external electrode system (Gecor<sup>®</sup>), was used for monitoring the electrochemical parameters first in tension ties, and then in beams, as depicted in Figure 6. The SME used allows confining the measurement to a delimited area ( $S_{med}$ ) of the reinforcement. In addition, corrosion adapted for SFRC sensors, developed in the corrosion department of National Commission of Atomic Energy (CNEA),<sup>25</sup> were used for making complementary monitoring only in beams. The corrosion sensors record the parameters, above-mentioned, using a set of electrodes embedded in the cementitious matrix of beams. The working electrode is an 8 mm control steel bar, the same as used for reinforcement, which allows indirect monitoring of the progress of corrosion from inside the beam (Figure 6c). In all specimens, measurements were carried out before and after the immersion of specimens in solution tanks.

After opening each tension tie, in order to adjust electrochemical measurements, superficial extensions of attacks ( $S_{real}$ ) and maximum pitting penetrations ( $P_{PIT}$ ) were measured on the damaged rebars. Values of area coefficients ( $\alpha_S$ ), ratio  $S_{real}/S_{med}$ , were calculated. The current density ( $i_{CORR}$ ) was determined, using the calculated  $\alpha_S$ , and the average penetration ( $P_X$ ) was established considering the time ( $t$ ) of monitoring, according to Equation (1). Finally, pitting coefficients ( $\alpha_P$ ) were calculated according to Equation (2).<sup>6</sup> The calculated penetration values were compared with the penetrations measured in the reinforcements for assessing the accuracy of the criterion.

$$P_X = 0.0116 \times \frac{I_{CORR}}{\alpha_S \cdot S_{med}} \times t \quad (1)$$

$$\alpha_P = P_{PIT}/P_X \quad (2)$$

Using the results obtained from tension ties, monitoring of beams is being carried out considering the adjustments made for measurements with SME. Adjustments were also made in the setting of the electrochemical techniques used to carry out measurements with the sensors in search of more accurate measurements. It is worth mentioning that this experimental program assesses the corrosion during the propagation stage. The initiation stage is generally negligible when cracks are bigger than 0.10 mm.<sup>26</sup>

#### 4.1 | Situation scenario

After opening the tension ties, a common pattern of degradation was observed on the bottom face of the rebars (according to the pouring direction) coinciding with the crack location, as shown in Figure 7. An irregular, shape and length, corroded zone extended between 25 and 45 mm on each side of the crack location. Inside the degraded regions, pits of variable diameter and depth were observed, which generally coincided with defects in the SCI (voids). The length of the corrosion zone ( $l_{cz}$ ) and the maximum pitting depth ( $d_{pit}$ ) were measured by a digital caliber reading 0.01 mm and a digital dial

indicator reading 0.001 mm, respectively. Values of  $\alpha_S$ , (regarding the measurement area) and  $\alpha_P$  were calculated as aforementioned. Table 3 lists morphological characteristics of the attack at any cracks.

The described morphology is the result of the deterioration scenario generated by physical processes that the concrete undergoes prior to onset of corrosion:

- After casting, while the concrete has a plastic consistency, the combined action of concrete consolidation and exudation processes generates the formation of a vulnerable region, with lower quality paste (higher water/cement ratio), under the bottom face of reinforcing bars located in a horizontal position,<sup>27,28</sup> as depicted with blue color in Figure 8.

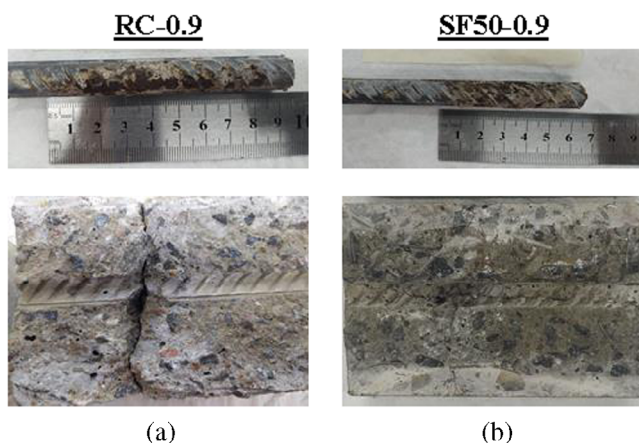


FIGURE 7 Morphology of the corroded rebars: in RC (a) and SF50 (b) tension ties.

- In the hardened state, during the application of loads, the mechanical stresses in the concrete generate damage to the concrete mass (formation of cracks) and to the SCI. Neighboring cracks, significant damage is generated in the SCI due to the movement that occurs when the cracks open (deformation). Larger crack openings can be associated with larger damage extensions on the SCI<sup>29,30</sup>
- In the physical scenario generated under the described context, the aggressive agents reach the reinforcement through the cracks, spread along the SCI damage. Finally, the corrosion process starts on the bottom face of the longitudinal rebars in coincidence with the damaged vulnerable region<sup>27,28,30</sup> (Figure 8).

In electrochemical terms, the corroded area acts as the anode, the surface of the steel without corrosion acts as the cathode, and the low-quality cementitious paste, in contact with the underside of the reinforcement, acts as the electrolyte since the ion flow conditions are more favorable than in the paste of the concrete mass.

The operating conditions of the equipment and the interference of metallic fibers generate the need to perform a correct interpretation of the values of the monitored electrochemical parameters:

- The presence of fibers in the cementitious matrix does not have a significant impact on the  $I_{CORR}$  and  $E_{CORR}$  measurements since they are recorded directly from the reinforcement and their values depend on the degradation state of the steel. Indeed, the recorded  $I_{CORR}$  values can be directly associated with the corroded zone (anode) inside the confined measurement region.

TABLE 3 Characteristics of the corroded rebars for each tension tie

Specimen	Crack		Corroded zone		Attack penetration		Coefficients	
	n°	Width (mm)	$l_{cz}$ (mm)	Area (cm <sup>2</sup> )	Average (mm)	$d_{pit}$ (mm)	$\alpha_S$	$\alpha_P$
RC-0.9	1°	<0.2	68	10.6	0.036	0.28	0.32	7.7
	2°	0.2	75	11.8	0.033	0.23	0.35	6.9
SF50-0.9	1°	<0.2	58	10.9	0.028	0.17	0.33	6.0
	2°	<0.2	56	8.8	0.035	0.32	0.26	9.2
RC-1.0	1°	0.2	72	11.3	0.034	0.22	0.34	6.5
	2°	0.3	71	13.4	0.029	0.24	0.40	8.3
SF50-1.0	1°	<0.2	55	8.6	0.035	0.18	0.26	5.2
	2°	<0.2	49	9.2	0.034	0.22	0.27	6.5
RC-1.1	1°	0.7	89	16.8	0.027	0.28	0.50	10.3
	2°	0.5	86	13.5	0.034	0.27	0.40	7.9
SF50-1.1	1°	0.2	53	10.0	0.038	0.29	0.30	7.6
	2°	0.2	60	11.3	0.034	0.20	0.34	5.9

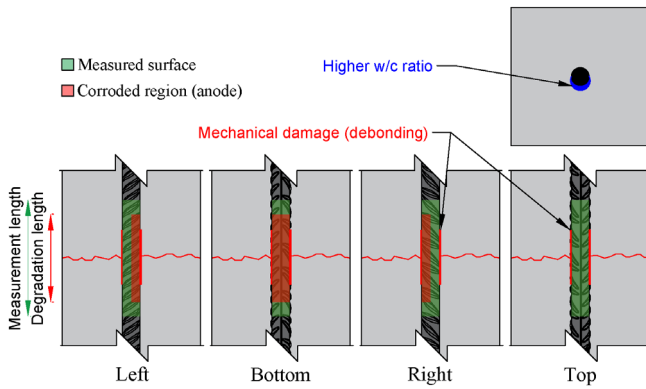


FIGURE 8 Degradation scenario at the intersection of reinforcement and cracks.

SME technology confines the measurement to a defined surface of the reinforcement. On the other hand, the internal sensors measure on the entire surface of the control electrode in contact with the concrete. If the relationship between the measuring surface of the equipment and the corroded area is known, in other words  $\alpha_S$ , the average section loss ( $P_X$ ) inside the corroded area can be calculated according to Equation (1). If pitting occurs in the inside the degraded region, its depth ( $P_{PIT}$ ) can be estimated by affecting the  $P_X$  value by a pitting factor ( $\alpha_P$ ) according to Equation (2).

- The measurement of  $\rho_M$ , on the other hand, represents the electrical resistance of the cementitious matrix located between electrodes with a known geometric configuration. In SME, the electrical resistance is recorded between the reinforcements (working electrode) and the counter electrodes of the equipment located on the surface of the concrete. That is, the electrical resistance of the cementitious matrix of the clear cover is recorded. In sensors, the electrical resistance between the control electrode (working electrode) and the counter electrodes of the sensor are recorded instead. That is, the electrical resistance of the cementitious matrix between the electrodes is recorded. In terms of the corrosion mechanism, the resistivity of the cementitious matrix is an indicator of the ionic conductivity through the electrolyte and is associated with the quality (i.e., water/cement ratio) of the cementitious paste. The presence of metallic fibers modifies the electrical behavior of the cementitious compound, making it more conductive, but does not modify the ionic conductivity of the cementitious matrix. Therefore, it is necessary to eliminate the influence of metallic fibers on resistivity measurements, in order to avoid erroneous conclusions about the corrosion susceptibility of reinforcements.

With the interpretation of the deterioration scenario and the operating conditions of the equipment, it is worth mentioning that:

- Knowing the relationship  $\alpha_P$ , measurements of  $I_{CORR}$  with SME, on the crack location, allow monitoring the corrosion on the lower face of reinforcement. With a commercial SME it is not possible to configure direct electrochemical techniques and it is necessary to correct resistivity values, eliminating the influence of the presence of metallic fibers, in order to perform an accurate evaluation of the resistivity of the cementitious matrix.
- Measurements with sensors should be interpreted based on their location with respect to cracks (Figure 6c):
  - When the location of the sensor and the crack coincide,  $I_{CORR}$  measurements allow to monitor the corrosion on the lower face of the witness electrode, knowing the relationship  $\alpha_P$ . With sensors it is possible to configure the electrochemical techniques to record the resistivity of the cementitious matrix, eliminating the influence of the presence of metallic fibers.
  - If the location of the sensor and the crack do not coincide,  $I_{CORR}$  measurements allow to monitor corrosion in a scenario where mechanical damage has no direct influence. Sensors located between cracks could be used to recognize the extent of mechanical damage, or the progress of contamination with aggressive agents, over time.

## 5 | RESULTS AND DISCUSSION

Figure 9 exhibits the monitoring of electrochemical parameters ( $i_{CORR}$ ,  $E_{CORR}$ , and  $\rho_M$ ) on tension ties during the wet-dry cycle period, respectively. The  $i_{CORR}$  values were calculated using an area coefficient ( $\alpha_S$ ) of 0.3, obtained as a general criterion from the analysis of the attack morphology. On  $\rho_M$  monitoring, the impact of steel fibers was observed and the matrix without fibers showed a higher resistivity, as expected. Figure 10 shows a comparison between  $i_{CORR}$  and  $\rho_M$  measurements, performed on RC and SF50 tension ties, respectively. It can be observed that  $i_{CORR}$  measurements show negligible influence despite the presence of steel fibers. Conversely,  $\rho_M$  measurements show a significant impact due to the steel fibers.

The interference of steel fibers in the measurements of resistivity was analyzed by several researchers.<sup>18,21,31</sup> The authors indicated the possibility of more accurately monitoring by using alternating current (AC) techniques. According to Berrocal et al.<sup>20</sup>, accurate values can be



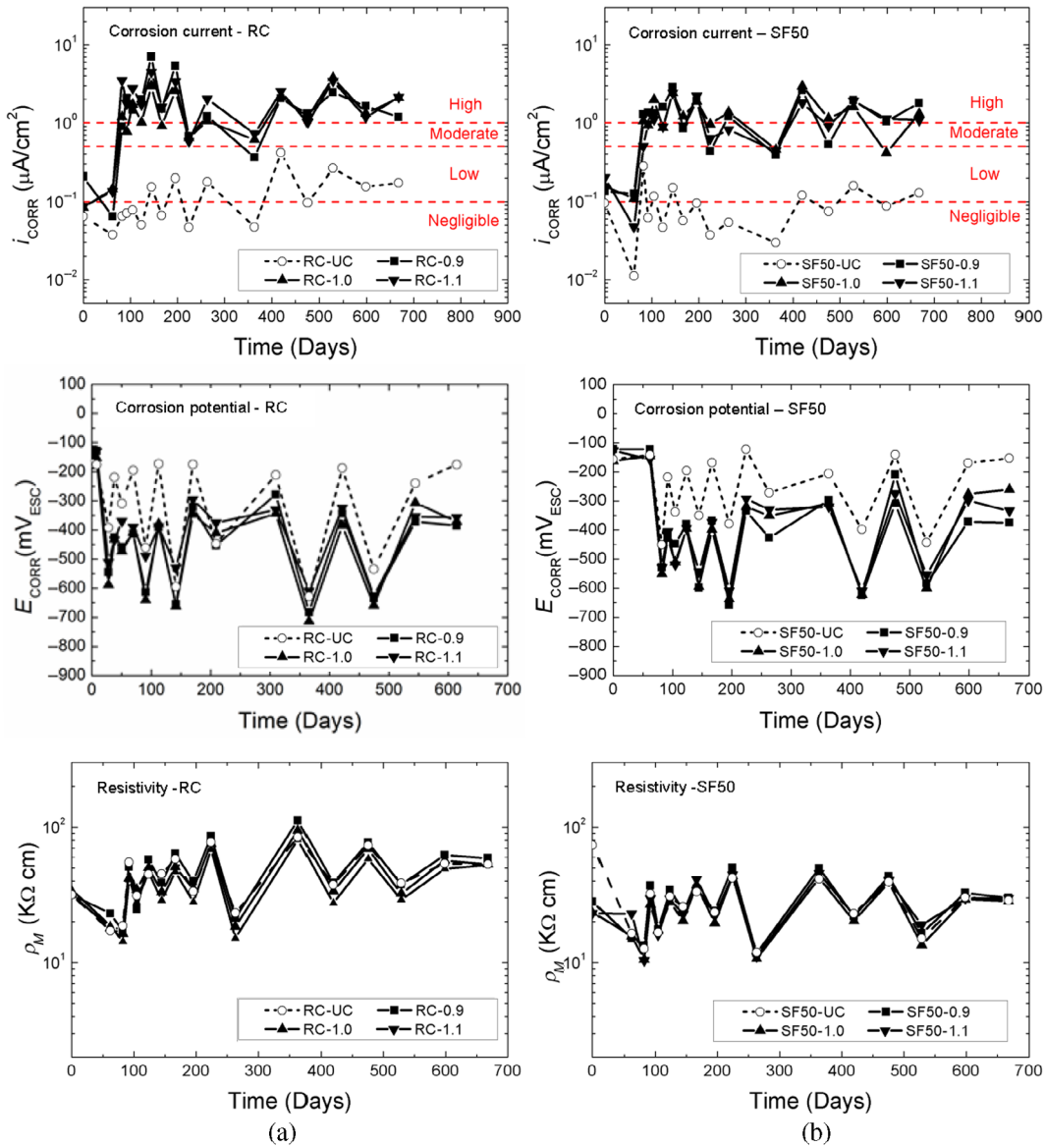


FIGURE 9 Electrochemical parameters ( $i_{CORR}$ ,  $E_{CORR}$ , and  $\rho_M$ ) monitoring in tension ties subjected to wet-dry cycles for: RC (a) and SF50 (b).

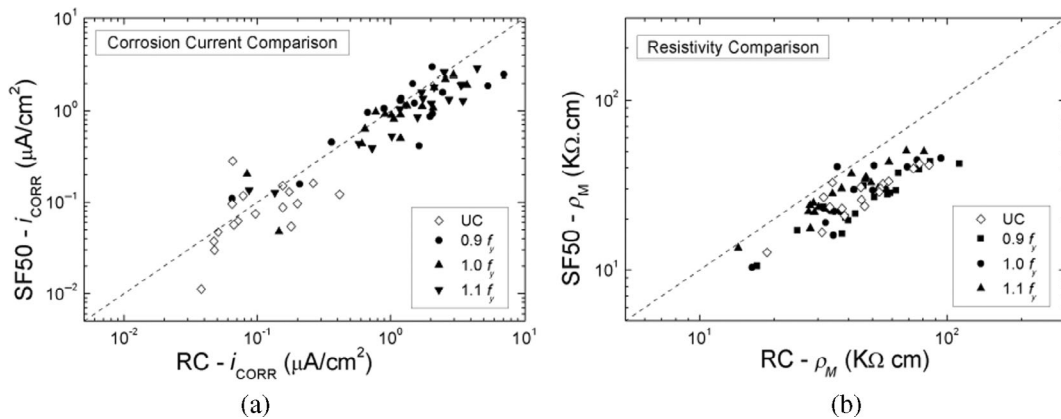


FIGURE 10 Comparison of RC and SF50 tension ties for  $i_{CORR}$  measurements (a), and  $\rho_M$  (b) measurements.

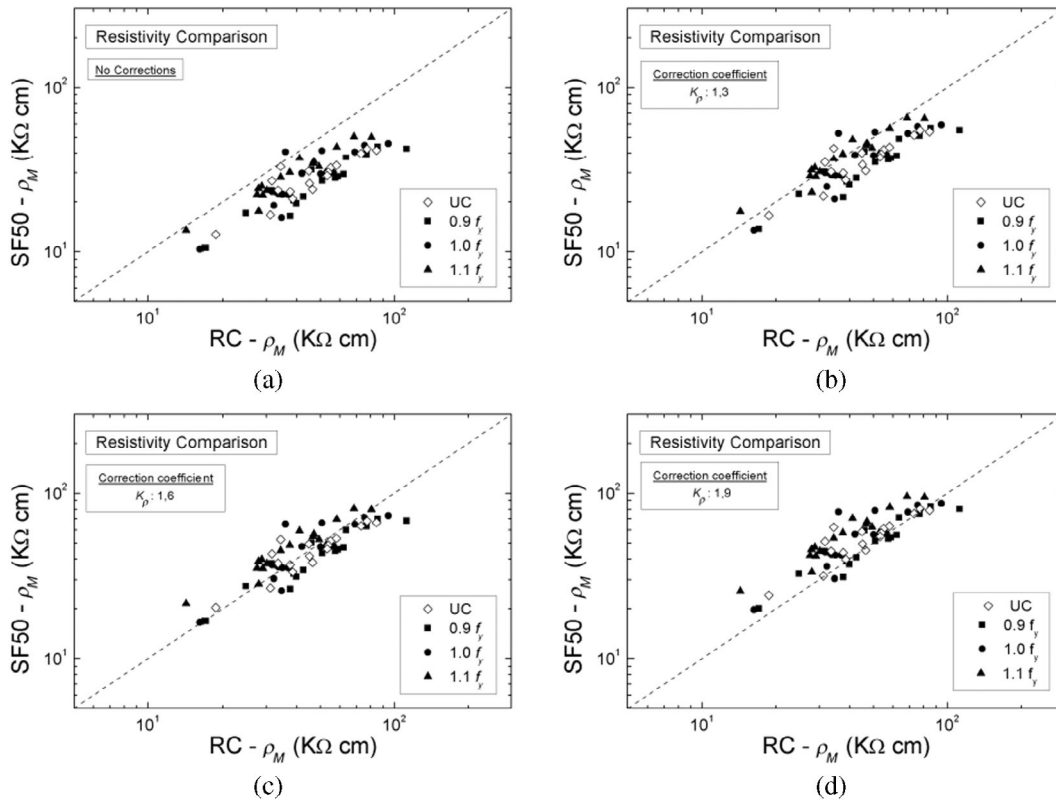


FIGURE 11 Match analysis between resistivity measurements, recorded with SME on RC and SFRC, using different correction coefficients. Match between  $\rho_M$  values using  $K_\rho = 1.0$  (“no correction”) (a),  $K_\rho = 1.3$  (b),  $K_\rho = 1.6$  (c), and  $K_\rho = 1.9$  (d).

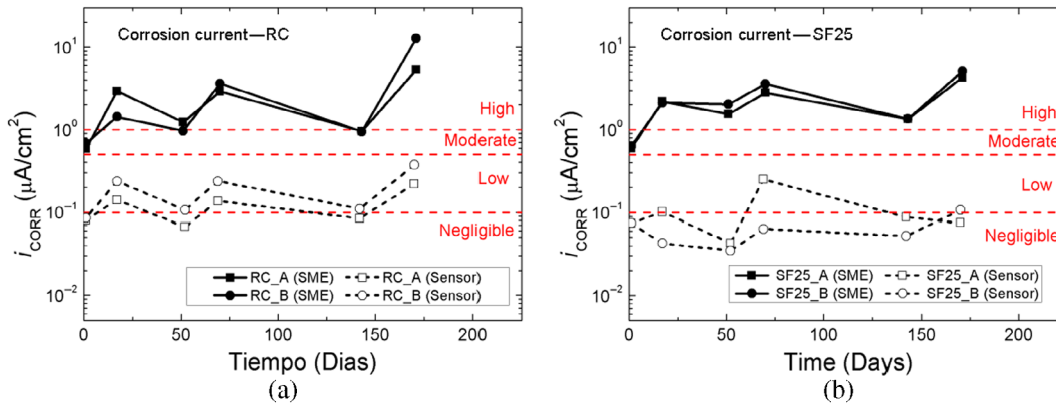
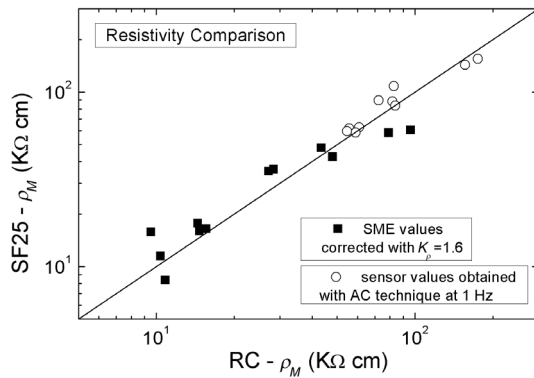


FIGURE 12 Electrochemical parameters monitoring in beams subjected to wet-dry cycles for RC (a) and SF25 (b).

obtained by using frequencies three orders of magnitude lower ( $\sim 1$  Hz) than the usual ones in RC ( $\sim 1000$  Hz). From resistivity measurements analysis on tension ties, correction coefficients ( $K_\rho$ ), for SME measurements, were established by direct match between RC and SF50  $\rho_M$  measurements, as shown in Figure 11. The  $K_\rho$  values, associated with types and doses of metallic fibers, must be established for each case, and used to adjust the resistivity measurements recorded with SME. The  $K_\rho$  value obtained in this paper is not directly applicable to other SFRC.

To make accurate monitoring of resistivity on beams, two methodologies for adjustments were applied:

- For SME measurements, a correction coefficient ( $K_\rho$ ) of 1.6, established from tension ties results analysis, was applied (Figure 11).
- For corrosion sensor measurements, a 1 Hz of frequency electrochemical impedance, was established as a technique for  $\rho_M$  measurements.



**FIGURE 13** Comparison between resistivity measurements of RC beams and SF25 beams, resistivity measurements adjusted by proposed methodologies. Values of  $\rho_M$  on SF25 recorded with corrosion sensor using AC technique at 1 Hz and values of  $\rho_M$  on SF25 recorded with SME corrected with a  $K_p = 1.6$ , as well.

Figure 12 shows the monitoring of  $i_{CORR}$  on beams, during wet–dry cycle exposition, by using SME and corrosion sensors. The  $i_{CORR}$  values were calculated using an area coefficient of 0.3, obtained as a general criterion from the analysis of the attack morphology on tension ties. The values recorded by the sensor are lower than those recorded by the SME. As previously mentioned, the difference is due to the fact that the sensor is not intercepted by cracks and therefore represents conditions of reinforcement deterioration not reached by mechanical damage.

For  $\rho_M$  measurements, the previously mentioned adjustments methodologies were applied. Figure 13 compares the average values of  $\rho_M$  recorded in RC and SF25 beams using corrosion sensors and SME. It can be observed that both applied methodologies improve the accuracy of the resistivity measurement.

Moreover, it is worth mentioning that during the experimental programs some interesting observations associated with the progress of the corrosion process were made:

- In all cases, the presence of a small crack, from 0.1 to 0.2 mm, influences the onset of corrosion. The corrosion process began in a short time, almost instantaneously, and oscillated between high and moderate degradation rates during wet–dry cycles.
- In tension ties, the cracks were wider than 0.2 mm since specimens were precracked up to the yielding load. Thus, no mitigation by sealing crack was observed in tension ties. Conversely, mitigation of degradation by sealing cracks was observed during the monitoring of beams. A smaller crack width (<0.2 mm), as occur under service loads, could be beneficial in the propagation stage making sealing of cracks more viable.<sup>32,33</sup>

- In terms of monitoring, the need to know the extension of the attack is notable for an accurate assessment of degradation. In longitudinal reinforcement, the deterioration in the zone of influence of the cracks showed a certain repetitive pattern that makes viable the use of  $\alpha_S$  to correct  $I_{CORR}$  measurements.
- For cracks at the yielding load of reinforcement (i.e.,  $\geq 0.2$  mm),  $\alpha_S$  values between 0.3 and 0.5 can be used at early ages of deterioration.
- Correspondence was observed between pitting and imperfections at the SCI; however, the  $\alpha_P$  values obtained do not allow general recommendations to be made. In order to define  $\alpha_P$  values, a more extensive study is required where different environmental conditions and SCI defects are considered. However, the values of  $\alpha_P$  around 10 will always be conservative.

## 6 | CONCLUSIONS

A practical approach was presented to monitoring the chloride-induced corrosion in RC and SFRC cracked elements. Different types of cracked specimens were subjected to wet–dry cycles in chloride solution, with 3% m/m of chloride ions (49.5 g/L of NaCl), and the progress of the corrosion process was characterized by electrochemical parameters monitoring and degradation morphology analysis. Based on the observation and obtained experimental results, the following conclusions can be drawn:

1. As expected, the presence of cracks has a high impact on the onset and development of corrosion. Even with crack widths smaller than 0.2 mm, corrosion initiation appeared in a very short time.
2. A common pattern of heterogeneous corrosion, at the crack location, was observed, and described. For monitoring of this scenario, values of  $\alpha_S$ , between 0.3 and 0.5, could be used to evaluate the deterioration generated by chloride attack and the presence of cracks.
3. The presence of fibers does not have a significant influence over  $I_{CORR}$  and  $E_{CORR}$  measurements. Metallic fibers only affect the  $\rho_M$  measurements. Correction factors, associated to types and doses of fibers, could be determined by direct match and should be used to improve the accuracy of registers made with SME. For monitoring with corrosion sensors, the use of AC techniques, at frequencies on the order of 1 Hz, improves the accuracy of  $\rho_M$  measurements.
4. Mitigation of degradation by sealing crack was observed during monitoring of specimens with small crack width (<0.2 mm) generated under service loads. In these cases, cracking control was the only

beneficial impact of fibers in corrosion process, making the sealing of cracks more viable.

## ACKNOWLEDGMENTS

The authors are grateful to technicians of the National Atomic Energy Commission (CNEA, Argentina) and the Multidisciplinary Training Laboratory for Technological Research (LEMIT, Argentina), for the assistance in performing the experimental program. The financial support of the Science, Technology, and Innovation Ministry of Argentina, through the National Found for Scientific and Technological Research (FONCYT, Argentina), is also acknowledged. Open Access Funding provided by Università degli Studi di Brescia within the CRUI-CARE Agreement.

## NOMENCLATURE

$\emptyset$	bar diameter
$c$	clear cover
$d_{\text{pit}}$	pit depth at the minimum cross-section
$E_{\text{CORR}}$	corrosion potential
$f_c$	mean value of the cylinder compressive concrete strength
$f_L$	mean value of the limit of proportionality
$f_{R,1}$	mean value of residual flexural tensile strength corresponding to CMOD = 0.5 mm
$f_{R,3}$	mean value of residual flexural tensile strength corresponding to CMOD = 2.5 mm
$f_y$	yield strength of reinforcement
$f_u$	ultimate strength of reinforcement
$I_{\text{CORR}}$	corrosion current
$i_{\text{CORR}}$	corrosion current density
$K_p$	correction coefficient
$l_{cz}$	length of corrosion zone at the crack
$P_{\text{max}}$	maximum load for the RC beam
$P_{\text{PIT}}$	maximum pitting penetration
$P_X$	average penetration
$S_{\text{med}}$	superficial measurement of a delimited area of the reinforcement
$S_{\text{real}}$	superficial extension of the attack
$w$	means crack width
$\alpha_p$	pitting coefficients
$\alpha_s$	area coefficients, the ratio of $S_{\text{real}}/S_{\text{med}}$
$\rho_{\text{eff}}$	effective reinforcement ratio
$\rho_M$	the resistivity of the cementitious matrix

## DATA AVAILABILITY STATEMENT

The data that support the findings of this study are available from the corresponding author upon reasonable request.

## ORCID

Antonio Conforti  <https://orcid.org/0000-0003-2796-7409>

## REFERENCES

- Bertolini L, Elsener B, Pedferri P, Redaelli E, Polder R. Corrosion of steel in concrete: prevention, diagnosis, repair. Weinheim: Wiley-VCH; 2013.
- Duffó GS, Farina SB. La corrosión de estructuras de hormigón armado: Principios básicos, monitoreo y prevención. 1st ed. Chisinau: Editorial Académica Española; 2016.
- Tuutti K. Corrosion of steel in concrete. Stockholm: Swedish Cement and Concrete Research Institute; 1982.
- François R, Arliguie G. Effect of microcracking and cracking on the development of corrosion in reinforced concrete members. *Mag Concr Res.* 1999;51:143–50. <https://doi.org/10.1680/mac.1999.51.2.143>
- El-Reedy MA. Concrete and steel construction: quality control and assurance. Boca Raton: CRC Press; 2017.
- Andrade C, Alonso C, Gulikers J, Polder R, Cigna R, Vennesland M, et al. Test methods for on-site corrosion rate measurement of steel reinforcement in concrete by means of the polarization resistance method. *Mater Struct Constr.* 2004; 37:623–43. <https://doi.org/10.1617/13952>
- Leporace-Guimil B, Conforti A, Zerbino R, Plizzari GA. Chloride-induced corrosion in reinforced concrete and fiber reinforced concrete elements under tensile service loads. *Cem Concr Compos.* 2021;124:104245. <https://doi.org/10.1016/j.cemconcomp.2021.104245>
- Mohammed UT, Otsuki N, Hisada M, Shibata T. Effect of crack width and bar types on corrosion of steel in concrete. *J Mater Civ Eng.* 2001;13:194–201.
- Otieno MB, Alexander MG, Beushausen HD. Corrosion in cracked and uncracked concrete - influence of crack width, concrete quality and crack reopening. *Mag Concr Res.* 2010;62: 393–404. <https://doi.org/10.1680/mac.2010.62.6.393>
- Wang J, Basheer PAM, Nanukuttan SV, Bai Y. Influence of cracking caused by structural loading on chloride-induced corrosion process in reinforced concrete elements: a review. In: Andrade C, Gulikers J, Polder R, editors. Durability of reinforced concrete from composition to protection. Switzerland: Springer; 2015. p. 99–113. [https://doi.org/10.1007/978-3-319-09921-7\\_10](https://doi.org/10.1007/978-3-319-09921-7_10)
- Arya C, Ofori-Darko FK. Influence of crack frequency on reinforcement corrosion in concrete. *Cem Concr Res.* 1996;26:345–53. [https://doi.org/10.1016/S0008-8846\(96\)85022-8](https://doi.org/10.1016/S0008-8846(96)85022-8)
- Schiessl P, Raupach M. Laboratory studies and calculations on the influence of crack width on chloride-induced corrosion of steel in concrete. *ACI Mater J.* 1997;1:56–61.
- Castel A, Vidal T, François R, Arliguie G. Influence of steel-concrete interface quality on reinforcement corrosion induced by chlorides. *Mag Concr Res.* 2003;55:151–9. <https://doi.org/10.1680/mac.2003.55.2.151>
- Zhang W, François R, Yu L. Influence of load-induced cracks coupled or not with top-casting-induced defects on the corrosion of the longitudinal tensile reinforcement of naturally corroded beams exposed to chloride environment under sustained loading. *Cem Concr Res.* 2020;129:105972. <https://doi.org/10.1016/j.cemconres.2020.105972>
- Vandewalle L. Cracking behaviour of concrete beams reinforced with a combination of ordinary reinforcement and steel fibers. *Mater Struct Constr.* 2000;33:164–70. <https://doi.org/10.1007/BF02479410>
- Bischoff PH. Tension stiffening and cracking of steel fiber-reinforced concrete. *J Mater Civ Eng.* 2003;15:174–82.

17. Tiberti G, Minelli F, Plizzari G. Cracking behavior in reinforced concrete members with steel fibers: a comprehensive experimental study. *Cem Concr Res.* 2015;68:24–34. <https://doi.org/10.1016/j.cemconres.2014.10.011>
18. Berrocal CG, Lundgren K, Löfgren I. Corrosion of steel bars embedded in fibre reinforced concrete under chloride attack: state of the art. *Cem Concr Res.* 2016;80:69–85. <https://doi.org/10.1016/j.cemconres.2015.10.006>
19. Berrocal CG. Corrosion of steel bars in fibre reinforced concrete: corrosion mechanisms and structural performance (PhD Thesis). Chalmers University of Technology, Sweden; 2017.
20. Berrocal CG, Hornbostel K, Geiker MR, Löfgren I, Lundgren K, Bekas DG. Electrical resistivity measurements in steel fibre reinforced cementitious materials. *Cem Concr Compos.* 2018;89:216–29. <https://doi.org/10.1016/j.cemconcomp.2018.03.015>
21. Solgaard AOS, Carsana M, Geiker MR, Küter A, Bertolini L. Experimental observations of stray current effects on steel fibres embedded in mortar. *Corros Sci.* 2013;74:1–12. <https://doi.org/10.1016/j.corsci.2013.03.014>
22. Beeby AW. The prediction of cracking in reinforced concrete members (PhD Thesis). University of London; 1971.
23. Conforti A, Zerbino R, Plizzari GA. Influence of steel, glass and polymer fibers on the cracking behavior of reinforced concrete beams under flexure. *Struct Concr.* 2019;20:133–43. <https://doi.org/10.1002/suco.201800079>
24. Conforti A, Zerbino R, Plizzari G. Assessing the influence of fibers on the flexural behavior of reinforced concrete beams with different longitudinal reinforcement ratios. *Struct Concr.* 2020;22:1–14. <https://doi.org/10.1002/suco.201900575>
25. Duffó GS, Farina SB. Development of an embeddable sensor to monitor the corrosion process of new and existing reinforced concrete structures. *Construct Build Mater.* 2009;23:2746–51. <https://doi.org/10.1016/j.conbuildmat.2009.04.001>
26. Berrocal CG, Löfgren I, Lundgren K, Tang L. Corrosion initiation in cracked fibre reinforced concrete: influence of crack width, fibre type and loading conditions. *Corros Sci.* 2015;98:128–39. <https://doi.org/10.1016/j.corsci.2015.05.021>
27. Mohammed TU, Otsuki N, Hamada H, Yamaji T. Chloride-induced corrosion of steel bars in concrete with presence of gap at steel-concrete interface. *ACI Mater J.* 2002;99:149–56. <https://doi.org/10.14359/11707>
28. Soylev TA, François R. Quality of steel-concrete interface and corrosion of reinforcing steel. *Cem Concr Res.* 2003;33:1407–15. [https://doi.org/10.1016/S0008-8846\(03\)00087-5](https://doi.org/10.1016/S0008-8846(03)00087-5)
29. Suzuki K, Ohno Y, Srisompong S. Experimental study on internal cracking of partially prestressed concrete flexural members. Part 2: internal cracking characteristics. *J Struct Constr Eng.* 1986;365:9–19.
30. François R, Maso JC. Effect of damage in reinforced concrete on carbonation or chloride penetration. *Cem Concr Res.* 1988;18:961–70.
31. Mason TO, Campo MA, Hixson AD, Woo LY. Impedance spectroscopy of fiber-reinforced cement composites. *Cem Concr Compos.* 2002;24:457–65. [https://doi.org/10.1016/S0958-9465\(01\)00077-4](https://doi.org/10.1016/S0958-9465(01)00077-4)
32. Cuenca E, Tejedor A, Ferrara L. A methodology to assess crack-sealing effectiveness of crystalline admixtures under repeated cracking-healing cycles. *Construct Build Mater.* 2018; 179:619–32. <https://doi.org/10.1016/j.conbuildmat.2018.05.261>
33. Cuenca E, Serna Ros P. Autogenous self-healing capacity of early-age ultra-high-performance fiber-reinforced concrete. *Sustainability.* 2021;13(3061):1–19. <https://doi.org/10.3390/su13063061>

## AUTHOR BIOGRAPHIES



**Enzo Gomez**, Atomic Energy National Commission (CNEA), San Martin, Argentina; Argentine Catholic University (UCA), Buenos Aires, Argentina.  
enzogomez@cnea.gov.ar



**Bruno Leporace-Guimil**, Department of Civil, Environmental, Architectural Engineering and Mathematics (DICATAM), University of Brescia, Brescia, Italy.  
b.leporaceguimil@unibs.it



**Antonio Conforti**, Department of Civil, Environmental, Architectural Engineering and Mathematics (DICATAM) University of Brescia, Brescia, Italy.  
antonio.conforti@unibs.it



**Giovanni Plizzari**, Department of Civil, Environmental, Architectural Engineering and Mathematics (DICATAM), University of Brescia, Brescia, Italy.  
giovanni.plizzari@unibs.it



**Gustavo Duffó**, Atomic Energy National Commission (CNEA), San Martin, Argentina; National University of San Martin (UNSAM), San Martin, Argentina; National Council for Scientific and Technical Research (CONICET), Buenos Aires, Argentina.  
duffo@cnea.gov.ar



**Raul Zerbino**, Multidisciplinary Training Laboratory for Technological Research (LEMIT), La Plata, Argentina; National University of La Plata (UNLP), La Plata, Argentina; National Council for Scientific and Technical Research (CONICET), La Plata, Argentina.  
zerbino@ing.unlp.edu.ar

**How to cite this article:** Gomez E, Leporace-Guimil B, Conforti A, Plizzari G, Duffó G, Zerbino R. A practical approach for monitoring reinforcement corrosion in steel fiber reinforced concrete elements exposed to chloride rich environments. *Structural Concrete*. 2022. <https://doi.org/10.1002/suco.202200302>